Virtual Refrigerant Charge Sensor for Booster Refrigeration Systems ☆

Glenn Andreasen[a,*], Roozbeh Izadi-Zamanabadi[a,b], Jakob Stoustrup[b]

[a]Innovation lab, Danfoss A/S, 6430 Nordborg, Denmark
[b]Department of Electronic Systems, Aalborg University, 9220 Aalborg, Denmark

Abstract

In this paper a virtual refrigerant charge sensor (VRCS) for a booster refrigeration system with a receiver unit is developed and proposed. The VRCS estimates the liquid level in the receiver unit by utilizing a combined mass and energy balance equation for mapping the change in the receiver unit's time constant to the liquid volume in the receiver unit. The time constant for the receiver unit is found by utilizing the commonly available data in an online subspace identification method. The parameters estimated by the online subspace identification method are recast in a linear fractional transformation structure to identify parameter changes due to liquid volume change. Hence, the VRCS functions in a plug & play framework where only the initial relative filling level in the receiver is required to be known. Results from utilizing the VRCS on experimental data from a charge test conducted on a test setup located at Danfoss A/S are shown, where the VRCS shows an accurate estimation of the liquid level in the receiver. The results from the VRCS can be employed for: early prediction of low charge in the system, early detection of a too large leakage rate, estimation of the current liquid level in the receiver on a daily basis, and estimation of the amount of charge lost.

Keywords: plug & play, subspace identification, leakage, virtual sensor, refrigerant charge, refrigeration system

☆This work is supported by the Innovation Fond Denmark, 7038-00100B, Denmark.

*Corresponding author

Email addresses: ga@danfoss.com (Glenn Andreasen), riz@es.aau.dk (Roozbeh Izadi-Zamanabadi), jakob@es.aau.dk (Jakob Stoustrup)

1. Introduction

Refrigeration systems are complex dynamic systems with many interacting subsystems, where the dynamic/static characteristics depend on the physical components (e.g. valves, compressors, etc.), operating condition and configuration (e.g. with/without heat recovery, parallel compressors, etc.). Much of this essential information is not known prior to design of control oriented applications. Vinther (2014)

The uncertainty of the system's dynamic/static characteristics makes design of control oriented applications a challenging task. An appealing approach to designing fault detection and diagnosis applications is to utilize a data-driven method that estimates the system's underlying dynamics online, and then utilize these findings in a fault detection and diagnosis scheme. Hence, the fault detection and diagnosis scheme would ideally be applicable independently of the system and operating conditions.

Various faults can occur in a refrigeration system and one of the most significant is leakage (Behfar et al., 2017, 2019). Depending on location and physical configuration, supermarket refrigeration systems lose approximately between 11% to 30% of the total amount of the charge annually (Behfar et al., 2019; Francis et al., 2017). Furthermore, due to regulations for environmental protection, food safety and cost related to loss of charge, timely detection of loss of charge is a task of paramount importance.

Several approaches for charge diagnosis and/or estimation have been proposed. The majority of the proposed methods address the problem for systems with fixed physical configuration without a receiver unit. Furthermore, the majority of the existing methods utilize the superheat or subcooling at the evaporator or condenser unit for diagnosing undercharge or overcharge. The superheat and subcooling are most common since they are found to be the parameter with the largest correlation to the refrigerant charge for systems without a receiver. e.g. Tassou & Grace (2005) have developed a fault diagnosis scheme, which utilizes a neural network on the subcooling at the condenser unit for diagnosing undercharge or overcharge. However, it does not estimate the current refrigerant charge. Other more recently reported results, such as Eom et al. (2019); Han et al. (2019); Liu et al. (2017); Shi et al. (2018); Yu et al. (2018) have also applied various neural network methods on the superheat and/or subcooling to reach similar conclusions about the charge. Other methods for evaluating the refrigerant charge have also been conducted: The concept of a virtual refrigerant charge sensor (VRCS) was first introduced in the work of Li & Braun (2009). The method utilizes four temperature measurements (at the evaporator, condenser, liquid line and at compressor suction) on a vapor-compression cycle for drawing conclusions about the refrigerant charge. Another VRCS is described in the work of Kim & Braun (2013). This VRCS is based on an empirical equation which utilizes the subcooling. However, the authors state that it does not have sufficient precision for systems with an accumulator. The major drawback for the above methods is exposed when the refrigeration system has a receiver unit included, since the effect on the superheat or subcooling will not be apparent before the receiver unit has lost its liquid refrigerant (Hong et al., 2019).

This research activity aims at developing a VRCS in a plug & play framework, which is applicable for any booster refrigeration system with a receiver unit, as illustrated in section 2 Fig. 1. The contribution of this work is a VRCS for a booster refrigeration system with a receiver unit which enables the opportunity of:

- providing early detection of low charge,
- providing early detection of too large leakage rate,
- providing an estimate of the lost charge (which from a maintenance point of view is a very important issue), and
- providing an estimate of the current liquid level in the receiver on a daily basis.

These goals are achieved by utilizing online subspace identification for obtaining a data-driven model of the unknown supermarket refrigeration system. This data-driven model is utilized in a linear fractional transformation (LFT) structure, in order to separate changes in the parameters caused by changes in refrigerant charge and changes caused by other system changes. Information about the refrigerant charge is derived by relating the dynamics of the data-driven model to the mass and energy balance equations.

Subspace identification methods have shown promising results in generating data-driven models of CO_2 supermarket refrigeration systems as well as other complex systems, see e.g. Andreasen et al. (2019a,b); Chen et al. (2017); Sankar Rao & Chidambaram (2017); Vajpayee et al. (2018). Utilizing subspace identification models in a fault detection and diagnosis framework is a relatively new field that has been receiving increasing attention. However, only a few methods are applicable for online implementation. One of the challenges is to manage the potentially large amount of data used for training the model. This is especially a challenge for a local industrial controller unit with limited memory (Chen et al., 2017, 2016; Ding, 2014; Gil et al., 2015; Houtzager et al., 2009). An alternative to subspace identification is the prediction error method (PEM). PEM's are well defined for convex systems, but for non-convex systems they suffer from the risk of getting stuck in a local minimum (Katayama, 2006; Lennart, 1999).

The LFT structure has been extensively utilized for managing changes in parameters for various control oriented tasks (Farah et al., 2019; Tabatabaeipour et al., 2015; Jin & Yang, 2008; Zhao et al., 2011; Zhou et al., 1996). The ability to manage change in the individual parameters is an appealing property, which will be utilized in this research for tracking changes between the currently identified systems and the nominal system.

The remaining part of this paper is structured as follows: In section 2 the considered system is described. Section 3 describes the relation between the dynamics and the liquid volume in the receiver. Section 4 describes a reduced subspace identification method and section 5 describes an online updating of the reduced subspace identification. In section 6 the parameters from the subspace identification are structured in LFT form. Section 7 presents the results of applying the VRCS on experimental data and lastly, section 8 presents the main conclusions of this work.

Nomenclature

h	specific enthalpy ($J\ kg^{-1}$)
k	discrete time (*sample number*)
M	mass (kg)
$\dot{m}$	mass flow rate ($kg\ s^{-1}$)
N	rotational speed (RPM)
OD	opening degree (%)
P	pressure (Pa)
t	time (s)
T	temperature (^oC)
T_s	sample time (s)
U	internal energy (J), input Hankel matrix
V	volume (m^3)
Greek symbols	
ρ	density ($kg\ m^{-3}$)
τ	time constant (s)
Superscripts	
i	intermediate variable
l	number of outputs
m	number of inputs
T	transpose
Subscripts	
f	future
fau	fault
g	gas
gc	gas cooler
l	liquid
ln	liquid normalized
low	lower triangular matrix
LT	low temperature
LTe	low temperature at evaporator
MT	medium temperature
MTc	medium temperature at compressor
MTe	medium temperature at evaporator
nom	nominal
p	past
par	parameter
pr	pressure
rec	receiver
tot	total
ud	unit delays
uf	future inputs
up	past inputs
upp	upper triangular matrix
v	volume
yp	past outputs

2. The refrigeration system

In this section a brief overview of the relevant aspects of the refrigeration system and the selected configuration is given. The system considered is a booster refrigeration system. This type of refrigeration system varies in size and component types. However, in this specific case it is a R744 (CO_2) booster refrigeration system including five medium temperature (MT) display cases and two low temperature (LT) display cases. The combined maximum loads are 45 kW for MT and 20 kW for LT. The MT and LT display cases are illustrated in Fig. 1 as two single blocks. Furthermore, the measured values in Fig. 1, i.e. pressure, temperature, valve opening degree and rotational speed are denoted with P, T, OD and N respectively. Most of these measurements are utilized by controller schemes as described in the items below:

- Pressure before the high pressure valve (HPV) is controlled using the HPV.
- Temperature before the HPV is controlled using the gas cooler fan. Both the temperature and the pressure (mentioned in the prior bullet) are controlled to reach a desired subcooling/trans-critical point.
- Pressure in the receiver is controlled using the bypass valve (BPV).
- Superheat at MT and LT is controlled using the individual electronic expansion valve (EEV). The superheat is controlled to prevent liquid from entering the compressors.
- Suction pressure at the LT compressor pack is controlled using the LT compressor pack. The suction pressure determines minimum temperature in the LT display cases.
- Suction pressure at the MT compressor pack is controlled using the MT compressor pack. The suction pressure determines minimum temperature in the MT display cases.

These control objectives are fulfilled by several controller schemes, illustrated in Fig. (1) as PI controller schemes. The purpose of this system is to transfer heat from the display cases and emit the absorbed heat through the gas cooler. This purpose is realised by alternating the pressure of a refrigerant. Decreasing the pressure of a refrigerant results in a decrease in temperature and therefore allows the system to absorb heat from e.g. foodstuff. An increase in pressure causes an increase in temperature which allows the system to dispose of the absorbed heat to e.g. the outside air. The different colors in Fig. (1) illustrate different pressure levels, where blue is the lowest pressure level, yellow is MT pressure level, green is intermediate pressure level and red is the highest pressure level. The system has a 110 liter receiver unit for storing unused refrigerant, where a refrigerant level sensor (of type AKS 4100, Danfoss (Accessed August 14, 2020)) with approximately 2 percent measurement error is installed.

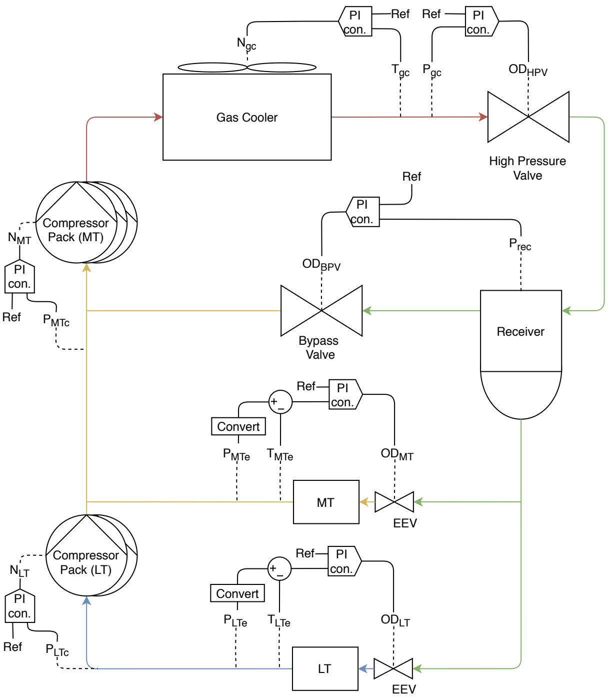

Figure 1: Illustration of the CO_2 refrigeration system and associated controllers and measurements.

3. Liquid level in the receiver

The unused refrigerant is supposed to be stored in the receiver unit. In some cases the refrigerant can get stuck in the gas cooler (due to low ambient temperature) if this happens the stuck refrigerant will not be available for cooling the goods. Thus, if there is no liquid in the receiver unit, the display cases will not have any liquid refrigerant available and as a result the system will suffer from low charge effects. In case the refrigerant is stuck in the gas cooler, a feature in the controller unit can be utilized for (ideally) moving all the refrigerant to the receiver unit. Hence, the liquid level in the receiver is utilized as a measurement (normally with a liquid level sensor) for obtaining information on the refrigerant charge in the system. When the charge of the system changes so does the mass (and energy) in the receiver unit, since the density of liquid and gas is different from one another. Thus, the receiver dynamics contains information on the refrigerant charge. In the following, the analysis of the receiver's dynamics using the mass and energy balance equations is described. The objective of the analysis is to capture the relation between the dynamics of the receiver and the liquid level in the receiver.

3.1. The mass balance equation

The mass balance for the receiver is found in a similar manner as in Andreasen et al. (2019a). In this paper the following assumptions are considered to be valid:

Assumption 1. *The gas in the receiver is assumed to be saturated.*

Assumption 2. *The liquid in the receiver is assumed to be saturated and incompressible.*

Assumption 3. *The mass and energy flow to the evaporators are assumed constant. Note: in practice this can be ensured by running the VRCS algorithm during the night where the load within the supermarket is constant.*

Assumption 1 allows the gas density (ρ_g), as well as the change in gas density in the receiver, to be found by utilizing the refrigerant properties. Assumption 2 allows the liquid density (ρ_l) in the receiver to be found by utilizing the refrigerant properties. Additionally, assumption 2 allows the change in liquid density as well as change in liquid specific enthalpy to be set to zero, however for transparency in the mass and energy balances this assumption is first applied when a certain constant is calculated, see Eq. (9). Assumption 3 reduce the number of variables and as an effect reduces complexity. The receiver unit with mass flows entering and leaving is illustrated in Fig. 2, where the refrigerant mass in the receiver is ($M_{rec} = M_g + M_l$). The change

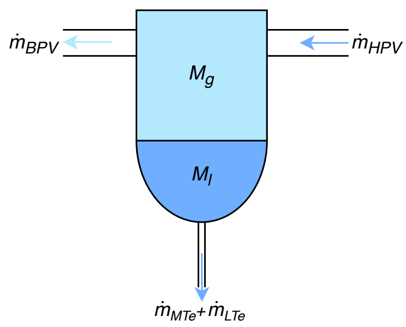

Figure 2: Illustration of the receiver unit with mass flows entering and leaving the receiver.

in refrigerant mass in the receiver depends on the difference between the mass flow entering and leaving the receiver. Thus, the change in mass in the receiver equals the mass flow entering the receiver from the HPV subtracted from the mass flows leaving the receiver through the BPV and through the EEVs:

$$\frac{d\,M_{rec}}{dt} = \dot{m}_{HPV} - \dot{m}_{BPV} - \dot{m}_{MTe} - \dot{m}_{LTe} \tag{1}$$

where Eq. (1) is known as the mass balance. The left hand side of Eq. (1) is expanded in terms of volumes (V_g, V_l), densities (ρ_g, ρ_l) and receiver pressure (P_{rec}):

$$\frac{d\,M_{rec}}{dt} = \frac{d\,(\rho_l V_l + \rho_g V_g)}{dt} =$$

$$\left(V_l \frac{d\,\rho_l}{dP_{rec}} + (V_{tot} - V_l)\frac{d\,\rho_g}{dP_{rec}}\right)\frac{d\,P_{rec}}{dt} + (\rho_l - \rho_g)\frac{d\,V_l}{dt} \tag{2}$$

The change in liquid volume term ($\frac{d\,V_l}{dt}$) is undesired since it is not measured. Thus, it is removed by combining the mass balance equation with the energy balance equation.

3.2. The energy balance equation

The following equation describes the energy balance for the receiver:

$$\frac{d\,U_{rec}}{dt} = \dot{m}_{HPV}h_{HPV} - \dot{m}_{BPV}h_{BPV} - \dot{m}_{MTe}h_{MTe} - \dot{m}_{LTe}h_{LTe}$$

i.e. the change in the receiver's internal energy, U_{rec}, is a function of the energy entering (through the HPV) and the energy leaving (through BPV as well as EEVs for MT and LT). The left hand side of the energy balance can be expanded as:

$$\begin{aligned}\frac{d\,U_{rec}}{dt} &= \frac{d\left(\rho_l V_l(h_l - \frac{P_{rec}}{\rho_l}) + \rho_g V_g(h_g - \frac{P_{rec}}{\rho_g})\right)}{dt}\\ &= \Bigg(V_l\rho_l\frac{d\,h_l}{dP_{rec}} + (V_{tot} - V_l)\rho_g\frac{d\,h_g}{dP_{rec}} + \\ &\qquad V_l h_l\frac{d\,\rho_l}{dP_{rec}} + (V_{tot} - V_l)h_g\frac{d\,\rho_g}{dP_{rec}} - V_{tot}\Bigg)\frac{d\,P_{rec}}{dt}\\ &\qquad + (\rho_l h_l - \rho_g h_g)\frac{d\,V_l}{dt}\end{aligned}$$

The aim is to utilize the energy balance to substitute the change in the liquid volume in the mass balance. Thus, the change in liquid volume is isolated:

$$\begin{aligned}\frac{d\,V_l}{dt} = &-\frac{\beta_{pr}}{\beta_v}\frac{d\,P_{rec}}{dt} + \frac{\dot{m}_{HPV}h_{HPV}}{\beta_v} - \frac{\dot{m}_{BPV}h_{BPV}}{\beta_v}\\ &- \frac{\dot{m}_{MTe}h_{MTe}}{\beta_v} - \frac{\dot{m}_{LTe}h_{LTe}}{\beta_v}\end{aligned} \tag{3}$$

where

$$\begin{aligned}\beta_{pr} &= \Bigg(V_l\rho_l\frac{d\,h_l}{dP_{rec}} + (V_{tot} - V_l)\rho_g\frac{d\,h_g}{dP_{rec}} + \\ &\qquad V_l h_l\frac{d\,\rho_l}{dP_{rec}} + (V_{tot} - V_l)h_g\frac{d\,\rho_g}{dP_{rec}} - V_{tot}\Bigg)\\ \beta_v &= (\rho_l h_l - \rho_g h_g)\end{aligned}$$

3.3. Main model: the combined energy and mass balance equation

The change in liquid volume is removed by substituting the energy balance, Eq. (3), into the mass balance, Eq. (2), :

$$\begin{aligned}&\left(V_l\frac{d\,\rho_l}{dP_{rec}} + (V_{tot} - V_l)\frac{d\,\rho_g}{dP_{rec}} - (\rho_l - \rho_g)\frac{\beta_{pr}}{\beta_v}\right)\frac{d\,P_{rec}}{dt}\\ &= \dot{m}_{HPV} - \frac{(\rho_l - \rho_g)\dot{m}_{HPV}h_{HPV}}{\beta_v} - \dot{m}_{BPV}\\ &+ \frac{(\rho_l - \rho_g)\dot{m}_{BPV}h_{BPV}}{\beta_v} - \dot{m}_{MTe} + \\ &\frac{(\rho_l - \rho_g)\dot{m}_{MTe}h_{MTe}}{\beta_v} - \dot{m}_{LTe} + \frac{(\rho_l - \rho_g)\dot{m}_{LTe}h_{LTe}}{\beta_v}\end{aligned} \tag{4}$$

Eq. (4) is for simplicity reformulated as Eq. (5) since the variable of interest is the change in dynamics in the combined energy and mass balance equation.

$$\begin{aligned}&\left(V_l\frac{d\,\rho_l}{dP_{rec}} + (V_{tot} - V_l)\frac{d\,\rho_g}{dP_{rec}} - (\rho_l - \rho_g)\frac{\beta_{pr}}{\beta_v}\right)\frac{d\,P_{rec}}{dt}\\ &= G(\dot{m}_{HPV}, \dot{m}_{BPV}, h_{HPV}, h_{BPV})\end{aligned} \tag{5}$$

where $G(\cdots)$ is a non-linear function. The dynamics of the receiver can be estimated by e.g. a linear identification method. Thus, the combined energy and mass balance, Eq. (5), is linearized:

$$\begin{aligned}\alpha\frac{d\,P_{rec}}{dt} &\approx C_1 P_{rec} \\ &\quad + g(\dot{m}_{HPV}, \dot{m}_{BPV}, h_{HPV}, h_{BPV}) + C_2,\\ \alpha &= \left(V_l\frac{d\,\rho_l}{dP_{rec}} + (V_{tot} - V_l)\frac{d\,\rho_g}{dP_{rec}} - (\rho_l - \rho_g)\frac{\beta_{pr}}{\beta_v}\right)\end{aligned} \tag{6}$$

where C_1, C_2 are constants and $g(\cdots)$ is a linear function at an operating point. The linear equation is utilized for investigating the time constant, which provides information on the liquid volume (V_l) in the receiver. The time constant can be found by taking the Laplace transform (s) of the linear equation from Eq. (6):

$$\begin{aligned}\alpha s P_{rec}(s) = C_1 P_{rec}(s) + &\\ g(OD_{HPV}(s), OD_{BPV}(s), P_{gc}(s),&\\ P_{MTc}(s), h_{HPV}(s), h_{BPV}(s))&\\ \Leftrightarrow&\\ (s - \frac{C_1}{\alpha})P_{rec}(s) = g(OD_{HPV}(s), OD_{BPV}(s), P_{gc}(s),&\\ P_{MTc}(s), h_{HPV}(s), h_{BPV}(s))&\end{aligned} \tag{7}$$

From Eq. (7) it is clear that the time constant is $\frac{\alpha}{C_1}$ (henceforth denoted τ_c). α is a known constant from which the liquid volume (V_l) can be estimated, given that the total receiver volume V_{tot} is known. C_1 is dependent on the operating point that includes the valve characteristics from the BPV and HPV, which makes it cumbersome to calculate. Hence, C_1 is regarded as an unknown constant. The time constant (τ_c) can be estimated by utilizing a linear system identification method. Thus, before the liquid level can be estimated the unknown constant (C_1) has to be removed. This is done by investigating the relative change in τ_c in percentage as:

$$\frac{\tau_{c,j}}{\tau_{c,nom}} = \frac{\frac{\alpha_j}{C_1}}{\frac{\alpha_{nom}}{C_1}} = \frac{\alpha_j}{\alpha_{nom}}$$

where $\tau_{c,nom}$, α_{nom} are the first estimates of τ_c and α, i.e. during nominal operation conditions. $\tau_{c,j}$, α_j are the jth estimation of τ_c and α. Then the liquid volume can be estimated as:

$$\begin{aligned}\frac{\tau_{c,j}}{\tau_{c,nom}} &= \frac{\alpha_j}{\alpha_{nom}}\\ &\Leftrightarrow\\ V_{l,j} &= (\frac{\tau_{c,j}}{\tau_{c,nom}} - 1)(V_{l,nom} + V_{tot}\zeta) + V_{l,nom}\end{aligned} \tag{8}$$

where:

$$\zeta = \frac{\frac{d\,\rho_g}{dP_{rec}} - \frac{\rho_l-\rho_g}{\rho_l h_l-\rho_g h_g}\beta_w}{\left(\frac{d\,\rho_l}{dP_{rec}} - \frac{d\,\rho_g}{dP_{rec}}\right) - \frac{\rho_l-\rho_g}{\rho_l h_l-\rho_g h_g}\beta_l}, \tag{9}$$

$$\beta_l = \rho_l \frac{d\,h_l}{dP_{rec}} + h_l \frac{d\,\rho_l}{dP_{rec}} - \rho_g \frac{d\,h_g}{dP_{rec}} - h_g \frac{d\,\rho_g}{dP_{rec}},$$

$$\beta_w = \rho_g \frac{d\,h_g}{dP_{rec}} + h_g \frac{d\,\rho_g}{dP_{rec}} - 1$$

Note, that when ζ is calculated, assumption 2 is applied. From the above equation it is clear that the total volume is required to compute the liquid volume. However, the requirement to know the total volume (V_{tot}) of the receiver can be removed by normalizing Eq. (8) as:

$$V_{ln,j} = \frac{V_{l,j}}{V_{tot}} = \frac{(\frac{\tau_{c,j}}{\tau_{c,nom}} - 1)(V_{l,nom} + V_{tot}\zeta) + V_{l,nom}}{V_{tot}}$$

$$V_{ln,j} = \left(\frac{\tau_{c,j}}{\tau_{c,nom}} - 1\right)(V_{ln,nom} + \zeta) + V_{ln,nom} \tag{10}$$

then, $V_{ln,j} \cdot 100$ yields the relative liquid volume. Thus, to estimate the liquid volume in the receiver, the nominal filling level in percent ($V_{ln,nom}$) and a repeated estimation of the receiver's time constant have to be obtained. Through the repeated estimation of the time constant both the nominal time constant ($\tau_{c,nom}$) and the current time constant ($\tau_{c,j}$) can be derived.

There are several system identification methods available, through which the time constant can be estimated. In this paper subspace identification is utilized as it does not suffer from the risk of getting stuck in a local minimum (like prediction error methods does) and as there exist numerical robust algorithm for the implementation (Katayama, 2006; Lennart, 1999).

4. Reduced subspace identification

To reduce the computational requirements for the subspace identification algorithm an auto regression moving average (ARMA) model is derived instead of the fully formed state space model. The following steps are performed to obtain the ARMA model, which consist of the first steps in a subspace identification algorithm. This method will be referred to as *reduced subspace identification*. The following first steps of the subspace identification method are inspired by Andreasen et al. (2019a); Lennart (1999) and references within.

Consider a discrete-time LTI system described by:

$$\begin{aligned} x(k+1) &= Ax(k) + Bu(k) + Ke(k) \\ y(k) &= Cx(k) + Du(k) + e(k) \end{aligned} \tag{11}$$

where $x \in \mathbb{R}^n$ is the state vector, $u \in \mathbb{R}^m$ is the input vector, $y \in \mathbb{R}^l$ is the output vector, $e \in \mathbb{R}^l$ is the innovation white noise vector and $A \in \mathbb{R}^{n\times n}$, $B \in \mathbb{R}^{n\times m}$, $C \in \mathbb{R}^{l\times n}$, $D \in \mathbb{R}^{l\times m}$ are constant matrices.

The following extended system equations can be derived by recursive substitution of Eq. (11).

$$Y_p = \Gamma X_p + P^d U_p + P^s E_p$$
$$Y_f = \Gamma X_f + P^d U_f + P^s E_f$$

where $P^s \in \mathbb{R}^{i\cdot l\times i\cdot l}$ and $P^d \in \mathbb{R}^{i\cdot l\times i\cdot m}$ are lower triangular toeplitz matrices. The superscripts d and s are denoting 'deterministic' and 'stochastic'. $\Gamma \in \mathbb{R}^{i\cdot l\times n}$ is the extended observability. U_f, U_p, Y_f, Y_p are block Hankel matrices which are obtained by using the input and output data as:

$$Y_p = \begin{bmatrix} y(1) & y(2) & \cdots & y(K) \\ y(2) & y(3) & \cdots & y(K+1) \\ \vdots & \vdots & \ddots & \vdots \\ y(i) & y(i+1) & \cdots & y(K+i-1) \end{bmatrix} \in \mathbb{R}^{i\cdot l\times K}$$

$$Y_f = \begin{bmatrix} y(i+1) & y(i+2) & \cdots & y(i+K) \\ y(i+2) & y(i+3) & \cdots & y(i+K+1) \\ \vdots & \vdots & \ddots & \vdots \\ y(2i) & y(2i+1) & \cdots & y(K+2i-1) \end{bmatrix} \in \mathbb{R}^{i\cdot l\times K}$$

where i and K are sufficiently large. $U_f \in \mathbb{R}^{i\cdot m\times K}$ and $U_p \in \mathbb{R}^{i\cdot m\times K}$ are derived similarly. The future and past state sequences are:

$$X_p = \begin{bmatrix} x(1) & x(2) & \cdots & x(K) \end{bmatrix}^T \in \mathbb{R}^{n\times K}$$
$$X_f = \begin{bmatrix} x(i+1) & x(i+2) & \cdots & x(i+K-1) \end{bmatrix}^T \in \mathbb{R}^{n\times K}$$

In Ding (2014) and Shafiei et al. (2015) it is shown that the future states (X_f) can be expressed using the past inputs and outputs as:

$$\begin{aligned} Y_f &= L_w W_p + L_u U_f + L_e E_f \\ &\approx L_w W_p + L_u U_f \\ &= L\begin{bmatrix} W_p \\ U_f \end{bmatrix}, \qquad W_p = \begin{bmatrix} U_p \\ Y_p \end{bmatrix} \end{aligned}$$

$L \in \mathbb{R}^{i\cdot l\times i\cdot(2\cdot m+l)}$ is then estimated by solving the least square problem:

$$\min_L \left\| Y_f - L\begin{bmatrix} W_p \\ U_f \end{bmatrix} \right\|_F^2$$

This least square problem can be minimized by utilizing RQ-decomposition as shown in Ding (2014):

$$\begin{bmatrix} W_p \\ U_f \\ Y_f \end{bmatrix} = \begin{bmatrix} R_{11} & 0 & 0 \\ R_{21} & R_{22} & 0 \\ R_{31} & R_{32} & R_{33} \end{bmatrix} \begin{bmatrix} Q_1^T \\ Q_2^T \\ Q_3^T \end{bmatrix}$$

where R is a lower triangular matrix and Q is an orthonormal matrix. The solution to the least squares problem is:

$$\begin{aligned} Y_f &= \begin{bmatrix} R_{31} & R_{32} \end{bmatrix} \begin{bmatrix} R_{11} & 0 \\ R_{21} & R_{22} \end{bmatrix}^{\dagger} \begin{bmatrix} W_p \\ U_f \end{bmatrix} \Leftrightarrow \\ Y_f &= L\begin{bmatrix} W_p \\ U_f \end{bmatrix} \end{aligned} \tag{12}$$

Notice, that the orthonormal matrix (Q) is not utilized. Normally, for subspace identification further effort would be conducted to reduce the order and derive the state space matrices.

However, at this point an ARMA model (i.e. L) is achieved which includes the discrete time constant. The ARMA model is also described in Ding (2014) where it is utilized as a residual generator. L is usually derived in an offline manner where a predefined amount of data is gathered before L can be estimated. From a commercial perspective it is impractical to utilize the procedure for deriving L in an offline manner as the amount of data required can be large. However, if the lower triangular matrix (R) is updated online the amount of required memory could be greatly reduced and the computational power would be distributed across each update as well. Thus, an online updating of the reduced subspace identification algorithm is introduced.

5. Online updating of the reduced subspace identification

In this section updating of the ARMA model is described. First, a short recap on how the QR-decomposition is updated online and then how it is utilized in the reduced subspace identification.

5.1. Online updating of QR-decomposition

The upper triangular matrix (R_{upp}) from the QR-decomposition can be updated online by utilizing householder transformation (Andrew & Dingle, 2014). The QR-decomposition of a matrix $H \in \mathbb{R}^{b \times c}$, where $b \geq c$ is:

$$H = QR_{upp} \Leftrightarrow$$
$$Q^T H = R_{upp}$$

where $R_{upp} \in \mathbb{R}^{c \times c}$ is an upper triangular matrix and $Q \in \mathbb{R}^{b \times c}$ is an orthonormal matrix. A block of rows $U \in \mathbb{R}^{q \times c}$ can be added to the upper triangular matrix:

$$\begin{bmatrix} R_{upp} \\ U \end{bmatrix} = \begin{bmatrix} Q^T H \\ U \end{bmatrix} = \begin{bmatrix} Q^T & 0 \\ 0 & I \end{bmatrix} \begin{bmatrix} H \\ U \end{bmatrix}$$

where I is the identity matrix. Then U can be eliminated by applying another orthonormal matrix (Q_h) as:

$$\tilde{R}_{upp} = \tilde{Q}^T \tilde{H} = Q_h^T \begin{bmatrix} R_{upp} \\ U \end{bmatrix} = \underbrace{Q_h^T \begin{bmatrix} Q^T & 0 \\ 0 & I \end{bmatrix}}_{\tilde{Q}^T} \underbrace{\begin{bmatrix} H \\ U \end{bmatrix}}_{\tilde{H}}$$

Thus, it is possible to append a block of rows to an upper triangular matrix (R_{upp}) and update it to find a new upper triangular matrix ($\tilde{R}_{upp}$). Note that, every row in R_{upp} larger than n is zero and can be removed for every update of R_{upp}. Hence, $R \in \mathbb{R}^{n \times n}$ has constant size in contrast to H which will grow as rows (measurements) are appended. Thus, the updating of the QR-decomposition utilizes less memory for online implementation/use than the standard QR-decomposition. It should be noted that the QR-decomposition can be used for calculating the lower triangular matrix R_{low} from the RQ-decomposition. E.g. consider the upper triangular matrix R_{upp} from the QR-decomposition:

$$R_{upp} = Q^T H$$

the lower triangular matrix R_{low} from the RQ-decomposition can be derived by applying the transpose on the QR-decomposition:

$$R_{low} = H^T Q$$

5.2. The online subspace identification algorithm

The basis of this online subspace identification algorithm is to apply the online/updating version of the QR-decomposition. Then, at any give point, a system model (L, from Eq. (12)) can be estimated by utilizing R_{low}. In this paper the online subspace identification is implemented as illustrated in the flowchart in Fig. 3, where Matlab® notation is utilized and the following matrix dimensions apply:

$$w_p = \begin{bmatrix} U_p \\ Y_p \end{bmatrix} \in \mathbb{R}^{m \cdot i + l \cdot i \times 1}$$
$$u_f \in \mathbb{R}^{m \cdot i \times 1}$$
$$y_f \in \mathbb{R}^{l \cdot i \times 1}$$
$$R \in \mathbb{R}^{2 \cdot i \cdot (m+l) \times 2 \cdot i \cdot (m+l)}$$
$$h \in \mathbb{R}^{2 \cdot i \cdot (m+l) \times 2 \cdot i \cdot (m+l)}$$

where w_p, u_f and y_f contains the newest measurements at the discrete time (k). The online subspace identification algorithm starts with filling a matrix (h) with the measurement (w_p, u_f and y_f) until it has reached a square structure (i.e. $h \in \mathbb{R}^{2 \cdot i \cdot (m+l) \times 2 \cdot i \cdot (m+l)}$). Then, the first R can be calculated and updated with every new sample (k). Through R, a system model can be obtained as shown in Eq. (12). The accuracy of the identified model will, among other factors, largely depend on the number of measurements utilized for generating the R matrix. However, calculating the R matrix in an online manner as presented here provides the opportunity to evaluate the estimated model for a relatively low computational cost. Note that the "reset" option in the flowchart, is a handle for clearing prior knowledge. If less than a full reset is desired the potentially large matrix Q has to be stored.

The online subspace identification algorithm estimates a linear model based on data from the system. However, since refrigeration systems are non-linear and are affected by disturbances, a structure that can manage parameter variations is required. This structure is furthermore utilized to distinguish between changes in the operating point conditions and changes in the liquid volume. To this end a linear fractional transformation (LFT) is utilized.

6. Linear fractional transformation structure

The above algorithm is utilized to derive a discrete time first order model with the pressure in the receiver as the output (P_{rec}). Hence, l and i are both one. The input(s) for the subspace identification are defined in section 7. Changes in the parameters of the nominal model are expected partially due to changes in the system's operating point and partially due to loss of refrigerant. Thus, knowledge about the leakage behavior is

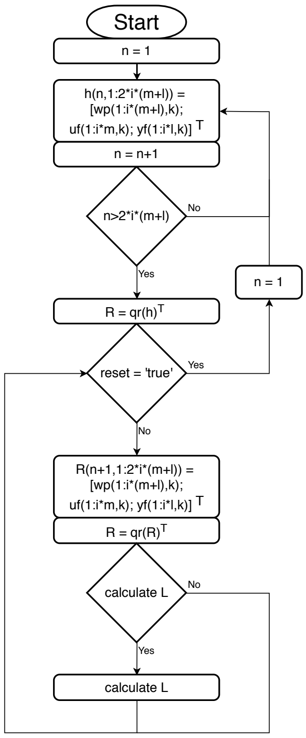

Figure 3: Flowchart of the online subspace identification algorithm.

adopted to sort out parameter changes due to loss of refrigerant. A refrigerant leak is expected to happen over a long period of time (more than a month) whereas the system change happens on a daily basis. Hence, the leakage can be isolated in the frequency domain. Thus, in the LFT structure a low pass and a high pass filter are incorporated on the parameters affecting the time constant. Change in the remaining parameters are also incorporated such that system changes are also accounted for. The nominal model (L_{nom}) with parameter and fault changes is denoted as the data-driven model (M). The data-driven model in the LFT structure is shown in Eq. (13) followed by the associated input (U) and output (Y). Reaching this structure of a model is also known as pulling out the delays (Zhou et al., 1996). Thereby, the system $Y = M \cdot U$ is obtained.

$$
\begin{aligned}
M &= \begin{bmatrix}
L_{up,nom} & L_{yp,nom} & L_{uf,nom} & I_{up,par} & \frac{T_s}{\tau_{fau}} + (1 - \frac{T_s}{\tau_{par}}) & I_{uf,par} & -1 + \frac{T_s}{\tau_{par}} & 1 - \frac{T_s}{\tau_{fau}} \\
I_{up,nom} & 0 & 0 & 0 & 0 & 0 & 0 & 0 \\
0 & I_{yp,nom} & 0 & 0 & 0 & 0 & 0 & 0 \\
0 & 0 & I_{uf,nom} & 0 & 0 & 0 & 0 & 0 \\
0 & 0 & I_{uf,nom} & 0 & 0 & 0 & 0 & 0 \\
0 & 0 & 0 & 0 & \frac{T_s}{\tau_{par}} & 0 & 1 - \frac{T_s}{\tau_{par}} & 0 \\
0 & 0 & 0 & 0 & \frac{T_s}{\tau_{fau}} & 0 & 0 & 1 - \frac{T_s}{\tau_{fau}}
\end{bmatrix} \qquad (13) \\
U^T &= \begin{bmatrix} o_{ud,up} & o_{ud,yp} & u_{LFT} & o_{par,up} & o_{par,yp} & o_{par,uf} & o_{ud,par,yp} & o_{fau} \end{bmatrix} \\
Y^T &= \begin{bmatrix} \hat{y}_{Prec} & z_{par,up} & z_{par,yp} & z_{par,uf} & z_{ud,up} & z_{ud,par,yp} & z_{fau} \end{bmatrix}
\end{aligned}
$$

In this expression, I denotes the identity matrix with appropriate dimension for the respective column. Note that the high pass filter is implemented by subtracting the filtered parameter from a low pass filtered version of the same signal. It is clear from M that $z_{par,uf}$ and $z_{ud,up}$ are equal to one another and therefore one of them could be omitted. However, both of them are kept in M such that the LFT structure is clearly shown, as seen in Fig. 4 where:

$$
\begin{aligned}
Z_{par}^T &= \begin{bmatrix} z_{par,up} & z_{par,yp} & z_{par,uf} \end{bmatrix} \in \mathbb{R}^{1\times 2\cdot m+1} \\
Z_{ud}^T &= \begin{bmatrix} z_{ud,up} & \hat{y}_{Prec} & z_{ud,par,yp} \end{bmatrix} \in \mathbb{R}^{1\times m+2} \\
Z_{fau} &= z_{fau} \in \mathbb{R}^1 \\
Y_{LFT} &= \hat{y}_{Prec} \in \mathbb{R}^1
\end{aligned}
$$

$$
\begin{aligned}
O_{par}^T &= \begin{bmatrix} o_{par,up} & o_{par,yp} & o_{par,uf} \end{bmatrix} \in \mathbb{R}^{1\times 2\cdot m+1} \\
O_{ud}^T &= \begin{bmatrix} o_{ud,up} & o_{ud,yp} & o_{ud,par,yp} \end{bmatrix} \in \mathbb{R}^{1\times m+2} \\
O_{fau} &= o_{fau} \in \mathbb{R}^1 \\
U_{LFT}^T &= u_{LFT} \in \mathbb{R}^{1\times m}
\end{aligned}
$$

and U_{upd} is a signal for updating the parameters. U_{SID} contains the measurements w_p, u_f and y_f from the subspace identification algorithm, see section (5). The loops around the LFT are closed by utilizing the following equations:

$$
\begin{aligned}
O_{fau} &= \Delta_{fau} \cdot Z_{fau} &&= z^{-1} \cdot Z_{fau} \\
O_{par} &= \Delta_{par} \cdot Z_{par} &&= (L_{nom} - L_j) \cdot Z_{par} \\
O_{ud} &= \Delta_{ud} \cdot Z_{ud} &&= z^{-1} \cdot Z_{ud}
\end{aligned}
$$

where z^{-1} is a unit delay and the linear models (L_j, L_{nom}) are provided by the subspace identification algorithm. The first

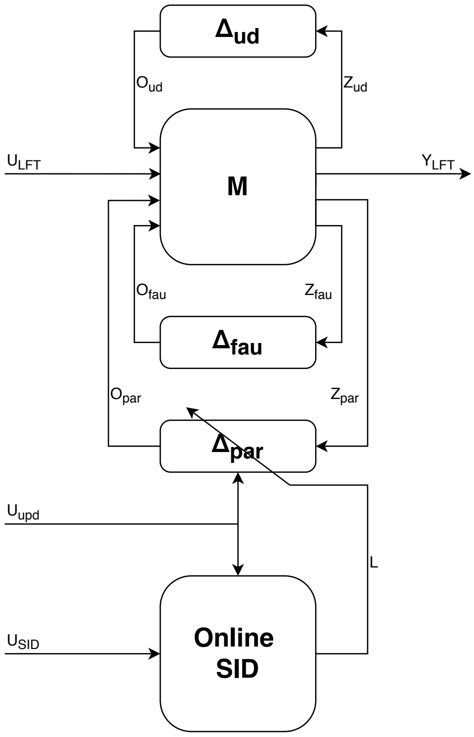

Figure 4: Illustration of the LFT structure with updating of the associated parameters.

identified model L_{nom} is stored. The L_j model is updated according to the training time. The training time is determined by the updating signal (U_{upd}), which utilizes the reset handle in the subspace identification algorithm. Thereby, removing prior knowledge. The signal Z_{fau} includes the parameter changes caused by changes in liquid volume. Z_{par} includes the parameter changes caused by fast changes in the operating point. Z_{ud} includes unit delays associated with the ARMA model and the low pass filter used for a high pass filter. In practice, the two filters in the LFT model are implemented with a slower sampling time to accommodate for their slow time constants (τ_{par}, τ_{fau}). This approach enhances numerical stability for the LFT model.

6.1. Estimation of the liquid level in the receiver unit

All the necessary information for estimating the liquid level in the receiver is available from the LFT structure. The continuous time constants can be found as:

$$\begin{aligned}\tau_{d,nom} &= L_{yp,nom}\\ \tau_{d,fau} &= L_{yp,j}\\ \tau_{c,fau} &= \frac{-T_s}{\log(\tau_{d,fau})}\\ \tau_{c,nom} &= \frac{-T_s}{\log(\tau_{d,nom})}\end{aligned}$$

then by using Eq. (10) the liquid level in the receiver can be calculated as:

$$\hat{V}_{ln} = \left(\frac{\tau_{c,f}}{\tau_{c,nom}} - 1\right) \cdot (V_{ln,nom} + \zeta) + V_{ln,nom}$$

where $\zeta = -0.9988$ for a receiver pressure of 36 bar.

7. Results

A 35 day long charge test was conducted on the system described in section 2. In this charge test the refrigeration system was charged rather than emptied. This is done since it was not possible to measure how much refrigerant was leaked from the system. The charge test was intended to start, where one of the display cases (MT and LT) was showing problems with keeping the required temperature for the goods. However, this starting point was very sensitive to whether there were liquid refrigerant in the receiver or not. Furthermore, the liquid sensor installed could not measure below 13 percent liquid level in the receiver. Thus, the test starts where one of the display cases were close to having problems with keeping the temperature. This scenario took place with an amount of 12 kg CO_2. The CO_2 system was then charged with 6 kg of CO_2 approximately every third day until it reached a liquid level in the receiver of 50 percent, which is roughly 50 kg. At the final step 12 kg of CO_2 was added. The final liquid level in the receiver corresponded to approximately 62 percent of the total volume. To excite the system dynamics a forth order pseudo random binary sequence (PRBS) signal with a sampling time of 200 seconds is added to the by-pass valve's opening degree signal.

The idea of the VRCS is to utilize the mean value of the first couple of estimated time constants as the nominal time constant (τ_{nom}) along with a provided nominal receiver filling level in percent ($V_{ln,nom}$). However, in this case the τ_{nom} is set manually by the authors, thereby eliminating the uncertainties of the initial guess of τ_{nom}. If there is a need to qualify the initial guess of the nominal receiver filling level, the VRCS could be combined with an existing leakage detection algorithm e.g. Fromm et al. (2018).

The input for the subspace identification algorithm is found through trial and error since the actuators (by-pass valve, high pass valve, gas cooler fans and compressors) often saturate during winter. Thus, utilizing the gas cooler pressure as the only input and receiver pressure as the output for the subspace identification was found to give persistently good estimation. The update signal is scheduled to reset the subspace identification algorithm every third hour. Thereby, accumulation of error over a long time period is avoided. The sampling time of the measurements as well as the sampling time for the identification algorithm is 5 seconds.

The result of utilizing the VRCS is shown in Fig. 5, where V_{ln} (blue signal) are measurements from a liquid level sensor and *Vl meas filt* (red signal) is a filtered version of V_{ln}. $\hat{V}_{ln}$ (yellow signal) is the output of the VRCS. The deviation between the VRCS and the filtered liquid level sensor in normalized root mean square error (NRMSE) is 0.33 which corresponds to a fit of 66 percent. This results in an accurate estimation of the liquid level on a daily basis. The continuous time constant ($\tau_{c,fau}$) range from 212 seconds at 57 percent liquid volume to 425 seconds at 14 percent liquid volume. Note that, the data where

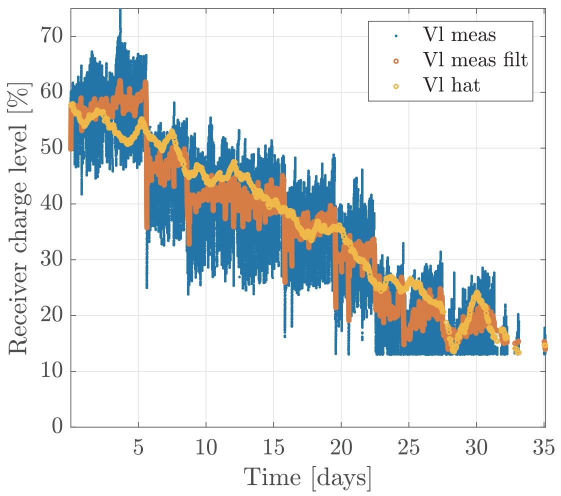

Figure 5: Illustration of the results from the VRCS, where *Vl meas* (blue signal) are measurements from a liquid level sensor (V_{ln}) and *Vl meas filt* (red signal) are a filtered version of *Vl meas*. *Vl hat* (yellow signal) is the output of the VRCS ($\hat{V}_{ln}$).

the liquid level sensor outputs a value below 13 percent is removed as the liquid level sensor yields false values (due to it's placement).

The deviations of the VRCS are suspected to be caused by the noise, disturbances, non-linearity, change in operating point, the assumptions made, and deviation in the sampling time. All of these factors influence the data that is utilized by the VRCS. Despite the uncertainties the VRCS output is always within the standard deviation of measured liquid level (V_{ln}) which is 13.5 percent.

Largely, there are two system operating conditions, which have the potential to cause deviations i.e. the ambient temperature and the system cooling load, since the operating points around the receiver are controlled as described in section 2. Deviation from controlled operating points only occurs briefly, hence these effects are mitigated by the filters implemented in the LFT structure. The effect from different cooling loads are reduced if not entirely removed by running the VRCS at night where the cooling loads on the refrigeration system are constant. Thus, only the ambient temperature, which causes the references for the gas cooler pressure and temperature to change is able to cause changes on the VRCS estimations at a frequency, which may be interpreted as the liquid volume changes.

The operating points for gas cooler pressure along with the receiver pressure are shown in Fig. 6 where changes in the gas cooler pressure (P_{gc}, in blue) can be seen. These deviations are partially due to changes in ambient temperature and partially due to the on/off switching of the compressors. The receiver pressure (P_{rec}, in red) shows small changes which are caused by the PRBS signal and the gas cooler pressure.

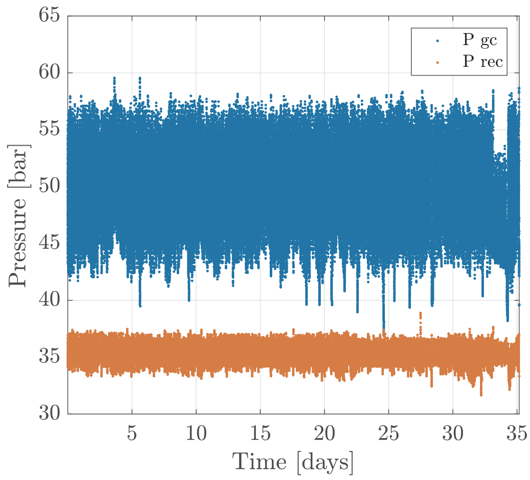

Figure 6: Illustration of the gas cooler pressure (*P gc*, in blue) and receiver pressure (*P rec*, in red).

The operating points for gas cooler temperature along with the ambient temperature are shown in Fig. 7, where changes in ambient temperature (T_{amb}, in red) are seen and therefore also changes in gas cooler temperature (T_{gc}, in blue) are observed.

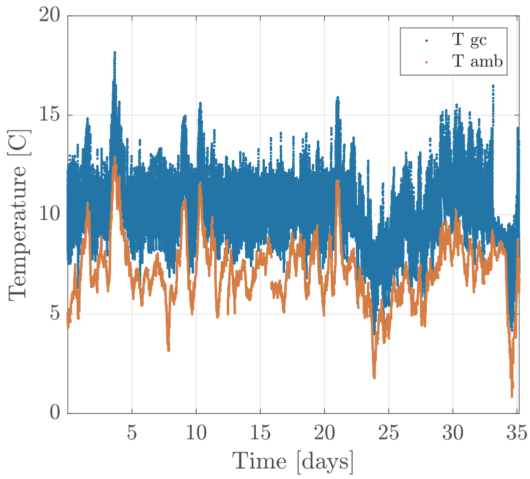

Figure 7: Illustration of the gas cooler temperature (*T gc*, in blue) and ambient temperature (*T amb*, in red).

Another important factor is the sampling time. The sample time between measurements can deviate since the logging of the measurements for the VRCS does not have priority. The VRCS expects/assumes a fixed sampling time of 5 seconds. Any deviation from this sampling time will have a direct impact on the estimated time constant. The upper plot in Fig. 8 shows the sampling time between each sample and the lower plot in Fig. 8 shows the probability histogram of the upper plot where only the three most significant sampling times are shown.

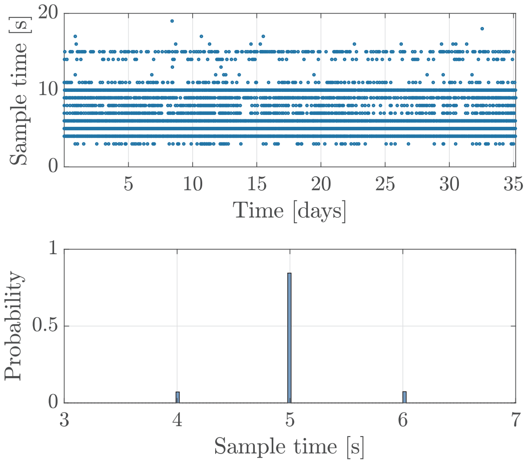

Figure 8: Illustration of the sampling time. The upper plot shows the sampling time between each sample. The lower plot shows a probability histogram of the upper plot, containing the three most significant sampling times.

8. Conclusions

In this paper a virtual refrigerant charge sensor (VRCS) for a booster refrigeration system has been proposed. The main innovation of the VRCS is the ability to sufficiently estimate the liquid level in the receiver unit which can be utilized for:

- providing early detection of low charge in a booster refrigeration system,
- providing early detection of a too large leakage rate in a booster refrigeration system
  - e.g. the rate of change in the liquid level can be evaluated each month,
- providing an estimate of the lost charge, and
- providing an estimate of the current change on a daily basis.

This VRCS utilizes the relation between the receiver unit's dynamic and the liquid refrigerant volume in the receiver unit. To this end, an online subspace identification algorithm and an LFT structure is utilized for repeated estimation of the receiver unit's dynamic and separating changes in the receiver unit's dynamic caused by refrigerant charge and by system operating condition. Furthermore, a combined energy and mass balance based equation is derived and utilized for mapping the estimated dynamic to the liquid refrigerant volume in the receiver. The VRCS is developed with a high plug and play potential as it is based on an online data-driven method and utilizes commonly available signals in commercial supermarket refrigeration systems. The prerequisite for the proposed method to perform appropriately is the information about the initial relative filling level in the receiver, i.e. $\frac{V_{l,nom}}{V_{tot}}$. This information can be provided by the field expert who is responsible for charging the refrigeration system. Thereby, the proposed framework offers an attractive and robust substitute for the existing liquid level measurement devices in the market.

References

Andreasen, G., Stoustrup, J., Izadi-Zamanabadi, R., Pardiñas, Á. Á., & Hafner, A. (2019a). Data-driven modeling of a CO_2 refrigeration system. In *2019 American Control Conference (ACC)* (pp. 5385–5390). IEEE.

Andreasen, G., Stoustrup, J., Pardiñas, Á. Á., Hafner, A., & Izadi-Zamanabadi, R. (2019b). Data-driven modelling of a R744 refrigeration system with parallel compression configuration. In *25th IIR International Congress of Refrigeration Proceedings*. International Institute of Refrigeration.

Andrew, R., & Dingle, N. (2014). Implementing qr factorization updating algorithms on gpus. *Parallel Computing*, *40*, 161–172.

Behfar, A., Yuill, D., & Yu, Y. (2017). Automated fault detection and diagnosis methods for supermarket equipment (rp-1615). *Science and Technology for the Built Environment*, *23*, 1253–1266.

Behfar, A., Yuill, D., & Yu, Y. (2019). Automated fault detection and diagnosis for supermarkets–method selection, replication, and applicability. *Energy and Buildings*, *198*, 520–527.

Chen, Z., Ding, S. X., Luo, H., & Zhang, K. (2017). An alternative data-driven fault detection scheme for dynamic processes with deterministic disturbances. *Journal of the Franklin Institute*, *354*, 556–570.

Chen, Z., Fang, H., & Chang, Y. (2016). Weighted data-driven fault detection and isolation: A subspace-based approach and algorithms. *IEEE Transactions on Industrial Electronics*, *63*, 3290–3298.

Danfoss (Accessed August 14, 2020). *Danfoss A/S - AKS 4100*. `https://www.danfoss.com/en/products/sensors-and-transmitters/dcs/liquid-level-sensors/`.

Ding, S. X. (2014). *Data-driven design of fault diagnosis and fault-tolerant control systems*. Springer.

Eom, Y. H., Yoo, J. W., Hong, S. B., & Kim, M. S. (2019). Refrigerant charge fault detection method of air source heat pump system using convolutional neural network for energy saving. *Energy*, *187*, 115877.

Farah, M., Mercère, G., Ouvrard, R., & Poinot, T. (2019). Combining least-squares and gradient-based algorithms for the identification of a co-current flow heat exchanger. *International Journal of Control*, *92*, 191–203.

Francis, C., Maidment, G., & Davies, G. (2017). An investigation of refrigerant leakage in commercial refrigeration. *International Journal of Refrigeration*, *74*, 12–21.

Fromm, J. M., Freiberg, N. et al. (2018). Detection of lack of refrigerant in a cooling system having multiple cooling locations. US Patent App. 15/986,863.

Gil, P., Santos, F., Palma, L., & Cardoso, A. (2015). Recursive subspace system identification for parametric fault detection in nonlinear systems. *Applied Soft Computing*, *37*, 444–455.

Han, H., Cui, X., Fan, Y., & Qing, H. (2019). Least squares support vector machine (ls-svm)-based chiller fault diagnosis using fault indicative features. *Applied Thermal Engineering*, *154*, 540–547.

Hong, S. B., Yoo, J. W., & Kim, M. S. (2019). A theoretical refrigerant charge prediction equation for air source heat pump system based on sensor information. *International Journal of Refrigeration*, *104*, 335–343.

Houtzager, I., van Wingerden, J.-W., & Verhaegen, M. (2009). Varmax-based closed-loop subspace model identification. In *Proceedings of the 48h IEEE Conference on Decision and Control (CDC) held jointly with 2009 28th Chinese Control Conference* (pp. 3370–3375). IEEE.

Jin, X.-Z., & Yang, G.-H. (2008). Robust fault-tolerant control systems design with actuator failures via linear fractional transformations. In *2008 American Control Conference* (pp. 4338–4343). IEEE.

Katayama, T. (2006). *Subspace methods for system identification*. Springer Science & Business Media.

Kim, W., & Braun, J. E. (2013). Performance evaluation of a virtual refrigerant charge sensor. *International journal of refrigeration*, *36*, 1130–1141.

Lennart, L. (1999). System identification: theory for the user. *PTR Prentice Hall, Upper Saddle River, NJ*, (pp. 1–14).

Li, H., & Braun, J. E. (2009). Development, evaluation, and demonstration of a virtual refrigerant charge sensor. *HVAC&R Research*, *15*, 117–136.

Liu, J., Li, G., Chen, H., Wang, J., Guo, Y., & Li, J. (2017). A robust online refrigerant charge fault diagnosis strategy for vrf systems based on virtual sensor technique and pca-ewma method. *Applied Thermal Engineering*, *119*, 233–243.

Sankar Rao, C., & Chidambaram, M. (2017). Subspace identification of unstable transfer function models. *Indian Chemical Engineer*, *59*, 1–20.

Shafiei, S. E., Knudsen, T., Wisniewski, R., & Andersen, P. (2015). Data-driven predictive direct load control of refrigeration systems. *IET Control Theory & Applications*, *9*, 1022–1033.

Shi, S., Li, G., Chen, H., Hu, Y., Wang, X., Guo, Y., & Sun, S. (2018). An efficient vrf system fault diagnosis strategy for refrigerant charge amount based on pca and dual neural network model. *Applied Thermal Engineering*, *129*, 1252–1262.

Tabatabaeipour, S. M., Stoustrup, J., & Bak, T. (2015). Fault-tolerant control of discrete-time lpv systems using virtual actuators and sensors. *International journal of Robust and nonlinear Control*, *25*, 707–734.

Tassou, S., & Grace, I. (2005). Fault diagnosis and refrigerant leak detection in vapour compression refrigeration systems. *International Journal of Refrigeration*, *28*, 680–688.

Vajpayee, V., Mukhopadhyay, S., & Tiwari, A. P. (2018). Multiscale subspace identification of nuclear reactor using wavelet basis function. *Annals of Nuclear Energy*, *111*, 280–292.

Vinther, K. (2014). *Data-driven control of refrigeration systems*. Ph.D. thesis Ph. D. thesis, Aalborg University.

Yu, F., Li, G., Chen, H., Guo, Y., Yuan, Y., & Coulton, B. (2018). A vrf charge fault diagnosis method based on expert modification c5.0 decision tree. *International Journal of Refrigeration*, *92*, 106–112.

Zhao, X., Yang, M., & Li, H. (2011). Decoupling features for fault detection and diagnosis on centrifugal chillers (1486-rp). *HVAC&R Research*, *17*, 86–106.

Zhou, K., Doyle, J. C., Glover, K. et al. (1996). *Robust and optimal control* volume 40. Prentice hall New Jersey.